www.serd.ait.ac.th/reric

Dynamic Performance Improvement of Wind Generation System Connected to a Multimachine Power System

M. Ahsanul Alam *[1] and A.H.M.A. Rahim*

Abstract – *A multimachine power system model including both induction and synchronous generators has been developed. The induction generator dynamics have been embedded in the general formulation as an equivalent synchronous machine through the slip dynamics term. The impact of connection of the induction generator through a weak as well as strong network connection is studied. For the induction generator, post-fault voltage recovery pattern in relation to received reactive power support from the grid is examined in the framework of multimachine power system. It is observed that a fast and adequate reactive power support is very important for the smooth recovery of induction generator terminal voltage. Improvement of dynamic performance of system through the introduction of a variable susceptance control circuit located at the induction generator terminal is investigated. Further enhancement of the dynamic performance with the introduction of additional PI control in the susceptance control circuit has been examined. The variable susceptance excitation scheme with auxiliary PI control is observed to provide very good transient performance. The proposed controller structure is very simple and employs signal local to each machine. It also performs in a robust manner.*

Keywords – Induction generator, multi-machine power system, PI control, reactive power support, wind energy.

1. INTRODUCTION

Due to growing environmental concern and escalating fuel price, generation of electricity using wind power has received significant attention worldwide in recent years [1]. A tendency to increase the amount of electricity generation from wind turbine can be observed in many countries and its importance is continuing to increase [2]. As the penetration level of wind power in power systems increases, the overall performance of the power grid will increasingly be affected by the characteristics of wind turbines. One of the major concerns related to the high penetration level of the wind turbines is the impact on power system stability. Therefore the assessment of the effects of wind power penetration to an existing power system necessitates the calculation of voltage and frequency profiles as well as examination of instability issues.

Induction generators consisting of squirrel-cage rotors are widely used as wind generators since they are relatively inexpensive, rigid, and require low maintenance. Studies show that they can even provide network damping [3]. But this kind of generators consume large amount of reactive power during normal operating condition. This consumption jumps sharply during grid fault due to large variation of slip. Instability in induction generator terminal voltage emerges from the deficiencies in the supply of demanded reactive power during the transient period. In recent years, a number of studies have been carried out to examine the possibility of maintaining system stability of power system with wind power infeed. These are basically blade pitch control (usually slow acting) on the turbine side and voltage, current, and power control on the generator side [4]-[8]. Braking resistor control for fault ride-through has been proposed in [6] to control active power during fault. Reactive power support during fault has also been proposed using various FACTS devices [8]-[10]. A combination of FACTS devices and braking resistor [11] or energy storage system [12] have also been proposed to have control on both active and reactive power. To achieve similar control, power electronics based energy capacitor system (ECS) has also been proposed recently [13]. Most of these studies dealt with either very simplified single machine infinite bus system (SMIB), or used various types of commercial power system dynamic simulation packages, PSS/E, PSCAD/EMTDC, DigSilent, etc. In general, the details investigation of the nature instability in the framework of multimachine power system is not available. Such investigations are essential to have an insight into the nature of the problem and look for appropriate remedies.

This article investigates the impact of connecting induction generator to a multimachine power system through a weak tie as well as strong tie. It also demonstrates the post-fault voltage recovery pattern in relation to the received reactive power support from grid. It is shown that incorporation of a variable susceptance excitation controller at the induction generator terminal can improve dynamic performance substantially.

2. DYNAMIC MODELING

The models for the different components of mixed wind generator and conventional power generation system with synchronous generator are given in the following:

2.1. *Wind Turbine Model*

The mechanical power output of a wind turbine is related to the wind speed V_ω by [14]:

$$P_m = \frac{1}{2}\rho A C_p(\lambda,\beta).V_\omega^3 \quad (1)$$

*Electrical Engineering Department, King Fahd University of Petroleum and Minerals, P.O. Box 692, Dhahran - 31261, Saudi Arabia.

[1] Corresponding author; Tel: + 966 860 1458, Fax: + 966 860 3535.
E-mail: mahsanul@kfupm.edu.sa

Here, ρ is the air density and A is the swept area by the turbine blades. The power coefficient C_p (λ,β) depends on both blade pitch angle β and tip speed ratio defined as:

$$\lambda = \frac{\Omega R}{V_w} \tag{2}$$

where, R is wind turbine rotor radius and Ω is the mechanical angular velocity. Expression for C_p is given by,

$$C_p(\lambda,\beta) = 0.5176\left(\frac{116}{\lambda_i} - 0.4\beta - 5\right)e^{\frac{-21}{\lambda_i}} + 0.0068\lambda$$
$$\frac{1}{\lambda_i} = \frac{1}{\lambda + 0.08\beta} - \frac{0.035}{\beta^3 + 1} \tag{3}$$

C_p can be obtained from a lookup table [15] or alternatively, by approximating through a non-linear function [16]. This study uses the second approach. Figure 1 shows C_p-λ curves for the pitch angle changing from 0 to 20° of a typical wind turbine used in this study. Figure 2 shows the corresponding power-speed characteristics curves for various wind velocities the speed being referred to generator side.

2.2. *Drive-Train Model*

Two-mass model is adopted here as much higher inertia wind turbine rotor is connected to the low inertia IG rotor with a relatively soft shaft [17], [18]. The dynamic equations of the two-mass representation is given by [19].

$$2H_t \frac{d\omega_t}{dt} = T_m - T_g - D_t\omega_t \tag{4}$$

$$2H_g \frac{d\omega_r}{dt} = T_g - T_e - D_g\omega_r \tag{5}$$

$$\frac{d\theta_s}{dt} = \omega_b(\omega_t - \omega_r) \tag{6}$$

The mechanical torque of the turbine rotor, T_m, and the mechanical torque applied to the generator rotor shaft, T_g, are given by:

$$T_m = \frac{P_m}{\omega_t} \tag{7}$$

$$T_g = K_s\theta_s + D_s(\omega_t - \omega_r)\omega_b \tag{8}$$

where θ_s is the shaft twist angle (in rad) , K_s is the shaft stiffness (in pu/elect. rad), and D is the damping coefficient (in pu.s/rad). The subscript t, g and s refer to the turbine and generator and shaft quantities respectively. T_e is the generator torque as given in Equation 14.

For a wind-farm, N turbines can be aggregated together as one singe turbine [20], giving the equivalent swing equation as:

$$2H^{agg}\frac{d\omega_r}{dt} = P_m^{agg} - P_e^{agg} \tag{9}$$

where, $H^{agg} = \sum_{i=1}^{N} H_i$; $P_m^{agg} = \sum_{i=1}^{N} P_{mi}$; and $P_e^{agg} = \sum_{i=1}^{N} P_{ei}$

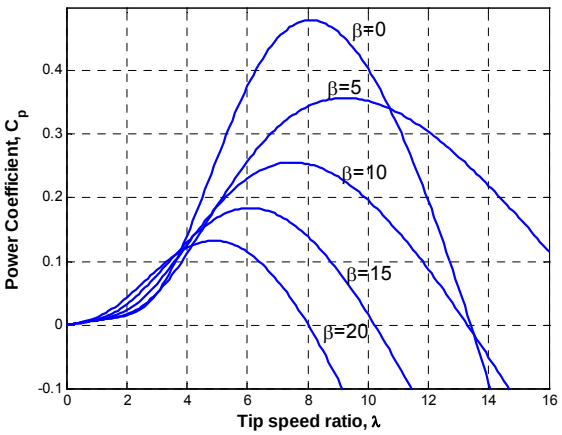

Fig. 1. Typical power coefficient–tip speed ratio plots.

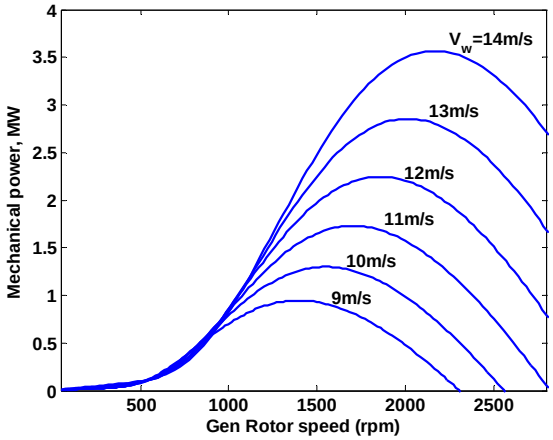

Fig. 2. Speed vs. power output characteristics of a wind turbine.

2.3. *Induction Generator Model*

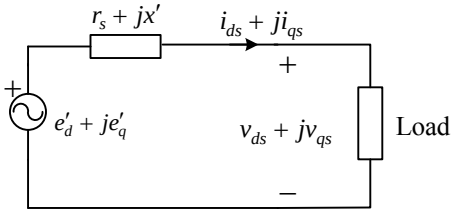

Fig. 3. Induction generator transient model.

The induction generator is modeled as an equivalent voltage source, $E' = e'_d + je'_q$, behind the transient impedance, $Z' = R_s + jx'$ as shown in Figure 3 [20]. It is represented by the third order model. Stator current and flux transients are neglected being very fast compared to rotor transients. This represents a good compromise between accuracy and simplicity [18], [21], [22].

The differential equations are then given by:

$$\dot{e}'_d = -\frac{1}{T'_o}[e'_d - (\frac{x_m^2}{x_m + x_r})i_{qs}] + s\omega_b e'_q \tag{10}$$

$$\dot{e}_q^{'} = -\frac{1}{T_o^{'}}[e_q' + (\frac{x_m^2}{x_m + x_r})i_{ds}] - s\omega_b e_d' \quad (11)$$

where, $x_{ss} = x_s + x_m$; $x' = x_s + \frac{x_m x_r}{x_m + x_r}$

$T_o' = \frac{x_m + x_r}{\omega_b R_r}$; $e_d' = -\frac{x_m}{x_m + x_r}\psi_{qr}$ and

$$e_q' = \frac{x_m}{x_m + x_r}\psi_{dr} \quad (12)$$

The symbols R, x, Ψ, ω, and *s* denote resistance, reactance, flux linkage, angular speed, and rotor slip respectively. The subscript s, r and b refer to the stator, rotor and base quantities respectively.

The stator voltages and currents are related through:

$$\left.\begin{aligned} v_{ds} &= -R_s i_{ds} + x' i_{qs} + e_d' \\ v_{qs} &= -R_s i_{qs} - x' i_{ds} + e_q' \end{aligned}\right\} \quad (13)$$

The electromagnetic torque is computed as:

$$T_e = e_d' i_{ds} + e_q' i_{qs} \quad (14)$$

The subscripts d and q stands for direct and quadrature axis values (in pu) respectively. The third differential equation is the swing equation, which is included in the drive-train model.

For N number of generators in a wind-farm, the electrical parameters of the equivalent machine are given by the following relations:

$$T_{oN}' = T_o'; \quad R_{sN} = \frac{R_s}{N}; \; x_{ssN} = \frac{x_{ss}}{N}; \; x_N' = \frac{x'}{N}; \quad (15)$$

In the above representation, reference axes (d-q) move at a speed ω_s (rad/sec) where as rotor move at a speed ω_r (rad/sec). This implies rotor axis makes an angle $\delta = (\omega_r t - \omega_s t)$ with respect to reference axis. Therefore,

$$\frac{d\Delta\delta}{dt} = -\Delta s\omega_b \quad (16)$$

2.4. *Synchronous Generator Model*

Neglecting stator transients, the synchronous generator is represented through the following 5th order model [23]:

$$\begin{aligned} \dot{e}_q' &= \frac{1}{T_{do}'}\left[E_{fd} - e_q' - (x_d - x_d')i_{ds}\right] \\ \dot{e}_d' &= \frac{1}{T_{qo}'}\left[-e_d' + (x_q - x_q')i_{qs}\right] \end{aligned} \quad (17)$$

$$\begin{aligned} \dot{\omega} &= \frac{1}{2H}\left[T_m - T_e - T_D\right]; \\ \dot{\delta} &= \omega_b \Delta\omega = \omega_b(\omega - 1) \\ \dot{E}'_{fd} &= \frac{1}{T_A}\left[K_A(v_{ref} - v_t) - E_{fd}\right] \end{aligned} \quad (18)$$

where,

$$\begin{aligned} T_e &= e_d' i_{ds} + e_q' i_{qs} + (x_q' - x_d')i_{ds} i_{qs} \\ T_D &= D_g(\omega - 1) = D_g \Delta\omega \end{aligned} \quad (19)$$

The stator voltage and currents are related through:

$$\left.\begin{aligned} v_{ds} &= -R_s i_{ds} + x_q' i_{qs} + e_d' \\ v_{qs} &= -R_s i_{qs} - x_d' i_{ds} + e_q' \end{aligned}\right\} \quad (20)$$

3. MULTIMACHINE POWER SYSTEM MODEL

A 4-machine 12-bus power system considered in this study as shown in Figure 4. The generation and load data for the base case are given in Appendix. The loads are represented by constant impedance and all network voltages and currents are written in common network reference frame [D-Q] rotating at synchronous speed. Eliminating all the load buses, the injected currents to the generator buses are written as:

$$I_{DQ} = Y_{red} V_{DQ} \quad (21)$$

where Y_{red} is the reduced admittance matrix, and V_{DQ} is the vector of generator bus voltage.

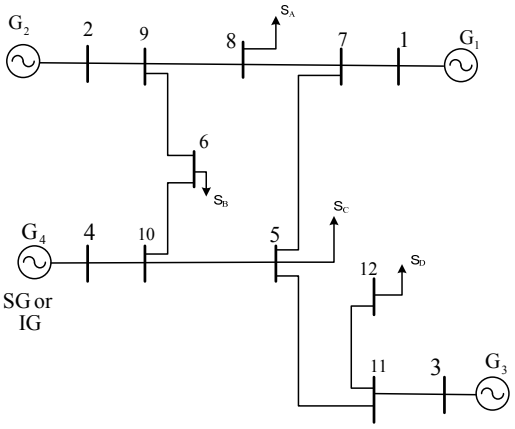

Fig. 4. Multimachine system configuration.

The quantities in dq frames of the individual generator, induction as well as synchronous, are related to the network frame DQ through:

$$[F]_{DQ} = [T][F]_{dq} \quad (22)$$

where $T = \begin{bmatrix} \sin\delta & \cos\delta \\ -\cos\delta & \sin\delta \end{bmatrix}$ and F may be either V or I.

Figure 5 shows the graphical representation of the relationship between the two reference frames.

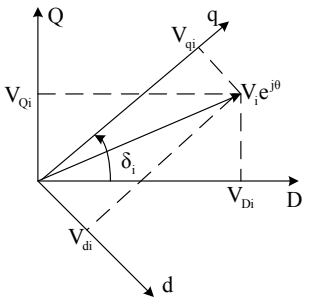

Fig. 5. Graphical representation of the relation between network (D-Q) and machine (d-q) reference frame.

The stator equations (Equations 13 and 20) for all machines can be written in matrix form as:

$$[V_{dq}]= [Z]I_{dq}+ E'_{dq} \quad (23)$$

where, V_{dq} is the vector of terminal voltages, I_{dq} is the vector of stator currents and E'_{dq} is the vector of e'_{dq}. Z is the impedance matrix whose elements are R_s and x' of the generators. I_{dq} in Equation 22 is obtained from:

$$I_{dq}=[T^{-1}Y_{red}T]V_{dq}=Y_mV_{dq} \quad (24)$$

where Y_m is the reduced admittance matrix transferred to machine (d-q) coordinates. Substituting Equation 24 back in Equation 23 yields:

$$I_{dq} = [1-Y_mZ]^{-1}Y_mE_{dq} \quad (25)$$

The block diagram in Figure 6 shows the conversion of variables between the two frames.

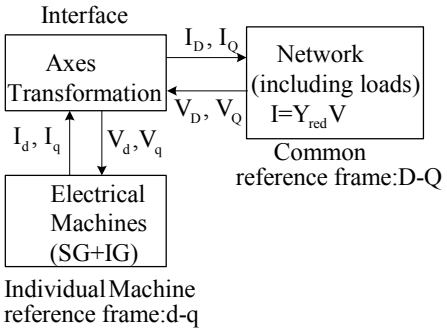

Fig. 6. Transformation from network (D-Q) to machine (d-q) reference frame.

Combining Equations 15, 16, and 24, the multimachine system can be expressed through one set of dynamic and another set of algebraic equation as:

$$\begin{aligned} \dot{x} &= f(x,z,u) \\ 0 &= g(x,z,u) \end{aligned} \quad (26)$$

where, x, z, and u are the state, algebraic, and input variables; f and g are the vectors of differential and algebraic equations, respectively. In this article, $x=[e'_d,e'_q,\omega,\delta,s,\omega_t,\theta_s,E_{fd}]^T$, $z=[i_d,i_q,v_t]^T$, and $u=[T_m,V_{ref},0,0]^T$.

4. SIMULATION RESULTS

The multimachine system shown in Figure 4 is simulated for studying the dynamic performance of the system. It is assumed that approximately 24% of the total generation is supplied by the wind farm which has 50 generators with capacity of 2 MW each. In the load flow analysis, the induction generator (IG) is represented as a PQ bus [24]-[26]. Steady-state analysis is performed to determine initial slip and reactive power consumed by the IG [19]. At the IG terminal appropriate reactive power is provided by a fixed capacitor. Then, with the obtained loadflow solution, the generators are initialized by solving its set of differential algebraic equations with all time derivatives set equal to zero. The simulation algorithm is shown in Figure 7 where the subscript ig refers to the quantities of induction generator. Y_{bf}, Y_{df} and Y_{pf} represents reduced Y_{bus} of the network at before fault, during fault and post fault respectively. All types of damping were disregarded to obtain worse scenario.

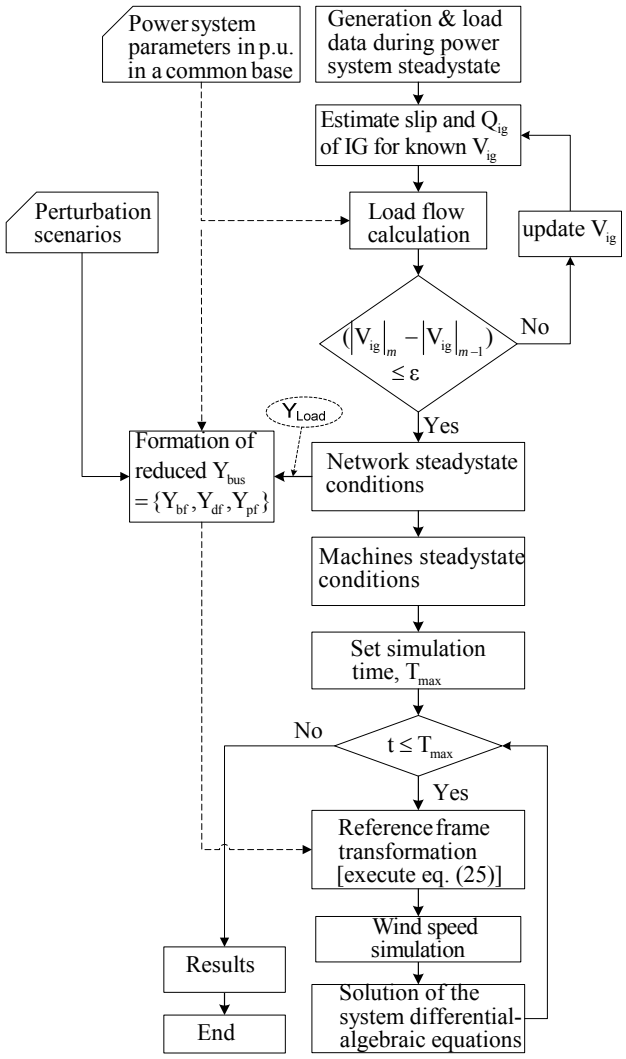

Fig. 7. Transient analysis algorithm for multimachine power system with windpower infeed.

For dynamic analysis, the following two cases were considered.

1. All the four machines in the system are synchronous generators.
2. Machine at bus # 4 is replaced by an equivalent induction generator

Two types of induction generator connections to the grid are considered. (i) A short circuit ratio (SCR) of 10.5 at the grid connection point (Bus 4) representing strong grid, and (ii) a SCR of 8.0 at bus 4 representing weak grid. To examine the influence of fault location, a bolted 3-phase fault was simulated at two locations, (a) at bus 6 and was cleared after 200 ms by tripping the line 6-10, denoted by fault F6, (b) at bus 5 and was cleared after 200 ms by tripping the line 5-10, denoted by fault F5.

For the fault F6, Figure 8 shows the terminal voltage response of the 4 generators when all of them are synchronous. Figure 9 shows the corresponding terminal voltage response when G4 is replaced by the equivalent induction generator. The above simulation results are for the case when tie 4-10 is strong ($Z_{4\text{-}10}$=0+j0.05 pu). Comparing both figures it is observed that there is not any appreciable change of voltage behavior when the induction generators were included in the system. In the case of IG, the voltage dips down to 0.25 pu due to slip dependence of rotor resistance. During the fault the speed

of the induction generator accelerates steeply. Increasing speed in a squirrel cage induction generator means increasing slip, s. From the equivalent circuit diagram of such an induction generator as shown in Figure 10, it can be seen that with increasing slip, s, the overall rotor resistance ($R_{rotor} = \frac{R_r}{s}$) decreases. As the slip continues to increase until the fault is cleared, the terminal voltage also continues to decrease. The gradual variation of slip causes corresponding variation in terminal voltage. The lower resistance also leads to more current flowing through the mainly inductive circuit of the generator, causing higher reactive power (Q) demand. Proper supply of this excess reactive power helps recovery of rotor flux linkage and the generator terminal voltage as will be seen in the following section.

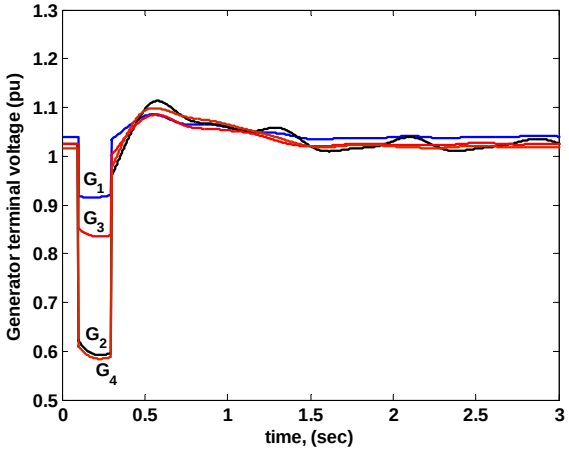

Fig. 8. Terminal voltage response with fault F6 when G4 is a synchronous generator (strong grid).

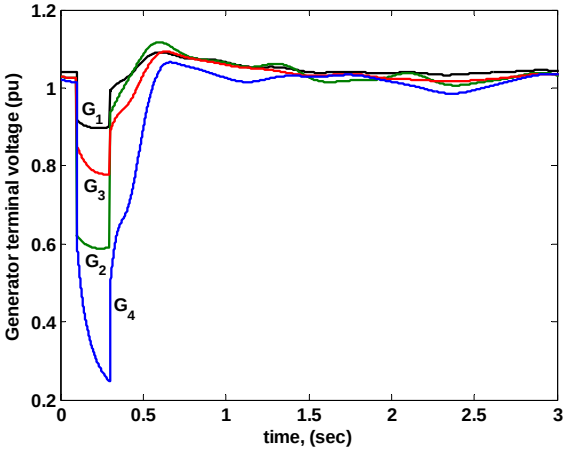

Fig. 9. Terminal voltage response with fault F6 when G4 is an induction generator (strong grid).

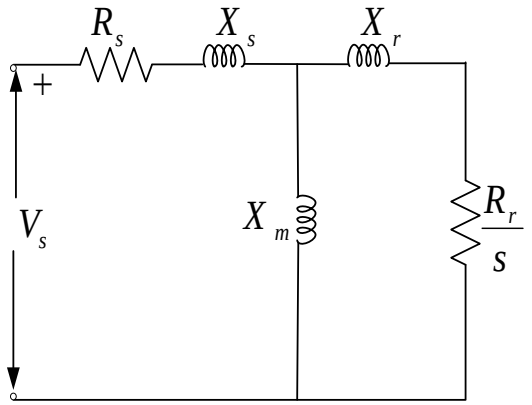

Fig. 10. Equivalent circuit diagram of squirrel cage induction generator.

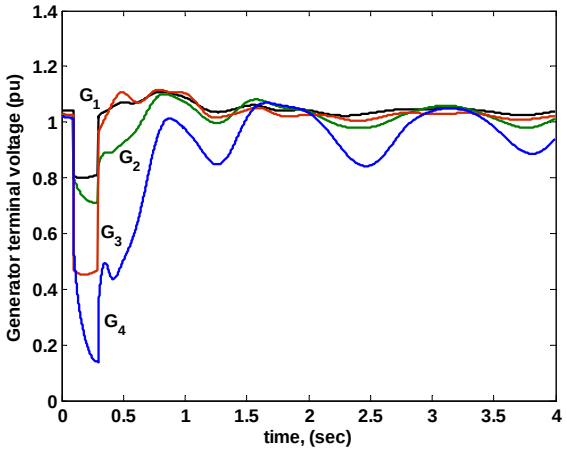

Fig. 11. Terminal voltage response with fault F5 and when G4 is an induction generator (strong grid).

For the same grid and fault F5, Figure 11 shows the terminal voltage response of G4 when it is an induction generator. It is seen that the voltage recovery is slower than the previous case. This is primarily attributed to the higher post fault network impedance that impedes necessary grid support to the induction generator.

Figure 12 shows the reactive power flow to/from the induction generator. It indicates that there is an obvious demand of excess reactive power in the post fault period for smooth recovery of induction generator terminal voltage. For the stronger grid with fault at bus 6 case, the demand for reactive power increases from 0.298 pu to 0.91 pu. Since the fixed capacitor at the IG terminal supplies only the steadystate demand (Q = 0.30pu), the excess Q should come from the grid supplied mainly by the swing generator G1. In the transportation period a substantial amount of Q is absorbed by the line reactance itself. This Q-loss in the line increases with the increase of line reactance. In the case of fault at bus 6, the transmission line connecting G1 and G4 has an impedance of Z_6 = 0.018+j0.2997 pu, where as for fault at bus 5 that is Z_5 = 0.027+j0.4005 pu. Figure 12 (b) shows that the Q support from the grid is not fast enough with required amount, which results in the slow recovery of IG terminal voltage as shown in Figure11.

For the weak grid case, the line reactance connecting bus 4 and 10 is increased to 0.25 pu and the same fault F6 is simulated and terminal voltage response is observed. Figure 13 shows the terminal voltage response when all 4 machines are synchronous generators. It shows that normal AVR restores the terminal voltage quickly. However, if G4 is an induction generator the voltage

recovery is further slows down as shown in Figure 14.

For the weak grid and fault F5, Figure 15 shows the terminal voltage response of G4 when it is an induction generator. It is seen that induction generator fails to recover its terminal voltage. Then, the electromagnetic torque (T_{em}) of induction generator drops suddenly as T_{em} is proportional to the square of the terminal voltage. But the mechanical torque of the wind turbine does not change rapidly during the short time interval. As a result, the induction generator accelerates rapidly due to large difference between the mechanical and electrical torques. The wind generator becomes unstable and requires to be disconnected from the power system. This temporary shutdown of induction generator may result in imbalance of generation and demand. In the absence of enough spinning reserve this may endanger the operation of other synchronous machines. From this it can be concluded that there is a minimum value of line strength below which IG will fail to recover its voltage in case of grid fault of certain level.

Figure 16 shows the comparison of level of reactive power support from the strong grid and weak grid. Figure 16 (c) shows that in the case of weak grid with fault at bus 6, the Q support from the grid is further reduced. Whereas with a fault at bus 5, IG receives a negligible amount of support from the grid as shown Figure 16 (d). This leads to eventual voltage collapse as shown in Figure 15. This indicates that there is a minimum grid strength under which SCIG operation is not possible without additional arrangement of Q support from the grid. The grid support should be fast enough with right amount for quick voltage recovery in the event of grid fault. In this regard a variable susceptance controller at the generator terminal is proposed.

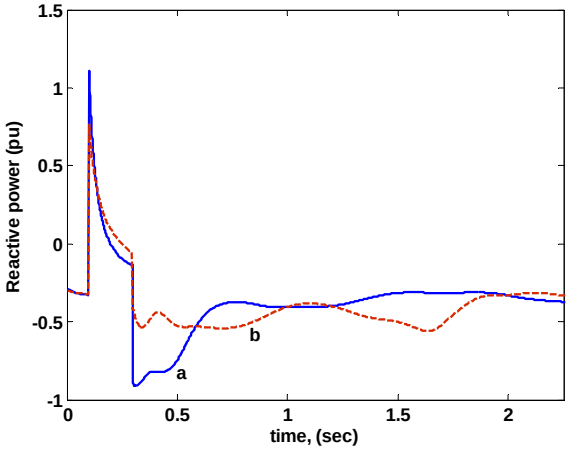

Fig. 12. Reactive power absorbed by the induction generator (strong grid) (a) fault F6 (b) fault F5.

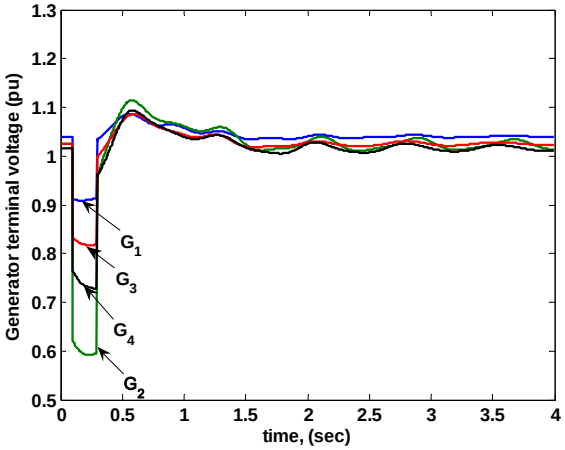

Fig. 13. Terminal voltage response with fault F5 when G4 is a synchronous generator (weak grid).

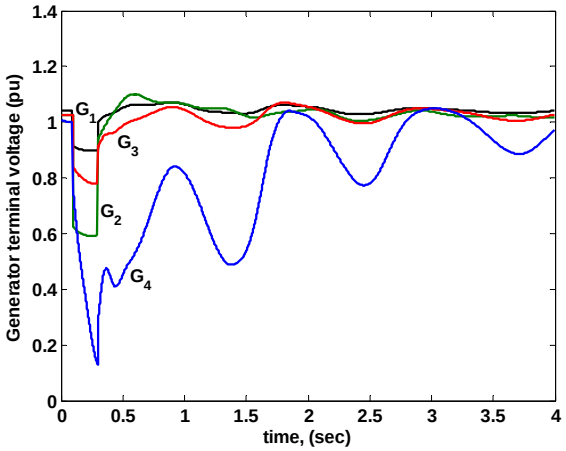

Fig. 14. Terminal voltage response with fault F5 when G4 is an induction generator (weak grid).

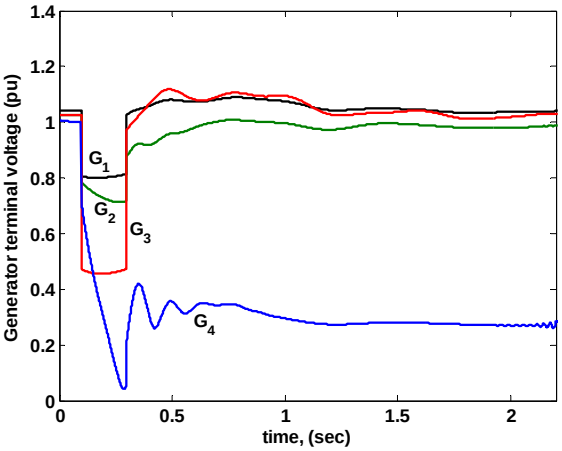

Fig. 15. Terminal voltage response with fault F5 when G4 is an induction generator (weak grid).

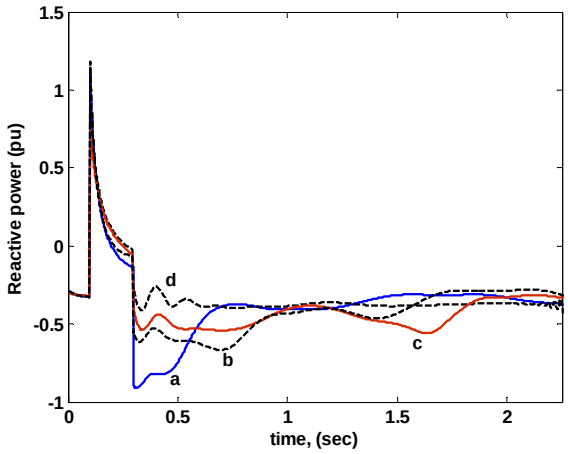

Fig. 16. Reactive power absorbed by the induction generator (a) strong grid, fault F6 (b) strong grid, fault F5 (c) weak grid, fault F6 (d) weak grid, fault F5.

5. THE PROPOSED CONTROLLER

The variable susceptance can be obtained by controlling a static VAR system through the firing angle control of the thyristors. The controller is connected to the grid side as shown in Figure 17. It contains a fixed capacitor (FC) needed for normal excitation of the induction generator. If additional capacitor excitation is required the thyristor switched capacitor (TSC) is switched in. A reduction in capacitance is achieved by switching in the thyristor controlled reactor (TCR) into the circuit. The equivalent inductive susceptance of the TCR, as a function of conduction angle σ, is given by [27]:

$$B_{TCR}(\sigma) = \frac{\sigma - \sin(\sigma)}{\pi X_{TCR}} \tag{27}$$

where X_{TCR} is the inductive reactance of TCR. The control range of the thyristor triggering delay angle α , is between π/2 and π, while the corresponding control range of the conduction angle σ =2(π-α) will be between π and 0. The TSC is switched ON when the output voltage of the induction generator (V_s) is less than the desired or reference value (V_{sr}) and the conduction angle of the TCR σ = 0 or the triggering delay angle α = π. For control purposes, the static VAR system described above is represented through a gain K_{SE} and time constant T_{SE} in the block diagram of Figure 18 [28].

Further enhancement of the transient profile may be achieved by introducing additional control (u) to the thyristor control circuit. Though various other controllers may have been used for generating the auxiliary control u, a PI has been used here because of its widespread use in industry and because of the ease in tuning its parameters. Figure 18 shows functional block diagram of the controller, including an additional PI controller with a washout. The washout is included to disable the additional control u under steady state conditions. The dynamic equations for the control block can be written as:

$$\frac{d\Delta B}{dt} = -\frac{1}{T_{SE}}\left[K_{SE}(V_s - V_{sr}) + \Delta B\right] + \frac{K_{SE}u}{T_{SE}} \tag{28}$$

The transfer function of the PI controller is:

$$G_c(s) = K_P + \frac{K_I}{s} \tag{29}$$

The input to the PI controller is variation of slip (Δs) and its tuned parameters are Kp= 3, Ki= 15, Tw=1.0. Detailed calculation steps Kp and Ki parameters using pole-placement technique is shown in [29], [30].

Figure 19 shows post-fault terminal voltage recovery with fault F6 when the induction generator connected with the weak grid is equipped with variable susceptance controller at its terminal. From Figure 19(b) it can be seen that there is a substantial improvement of post-fault terminal voltage response when variable susceptance controller is incorporated as compared to without it (Figure 19(a)). Note, the additional control u (Figure 18) has not been included here. The tuned value of controller's gain and time constant are K_{se} = 1.5, and T_{se} = 0.4, respectively. The controller compares the generator terminal voltage (V_s) with a reference signal (V_{sr}) and injects susceptance (ΔB) at the terminal, as may be necessary, to keep proper excitation of the system. Figure 20 shows the flow of reactive power to/from the induction generator. Introduction of variable susceptance controller enhances Q support to the induction generator terminal as depicted in Figure 20(a). Post-fault voltage profile is further enhanced with the introduction of additional control u through the incorporation of PI controller as shown in Figure 19(c). A voltage profile almost comparable to synchronous generators can be obtained. Figure 20(b) shows the corresponding Q-support to the induction generator.

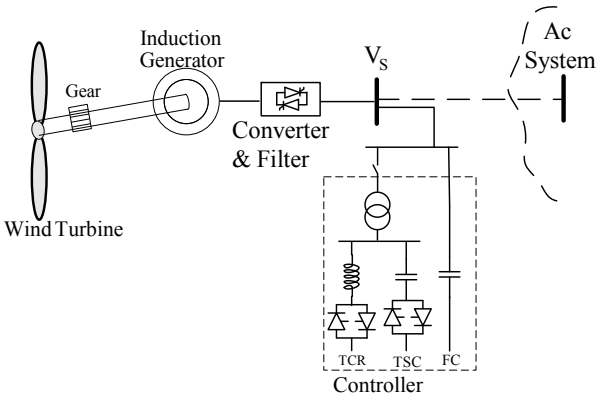

Fig. 17. Proposed controller configuration.

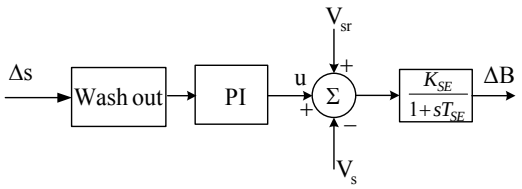

Fig. 18. Functional block diagram of the susceptance control.

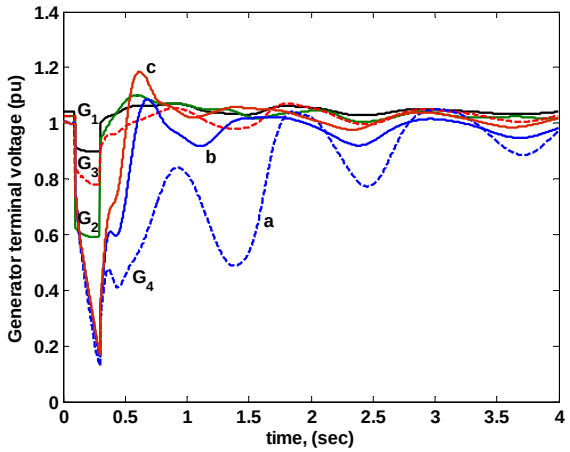

Fig. 19. Post-fault terminal voltage recovery of the induction generator with, (a) no susceptance control circuit, (b) with susceptance control circuit but no additional control u, and (c) with additional PI control in the susceptance control circuit. The induction generator is connected to the weak grid and fault F6 is applied.

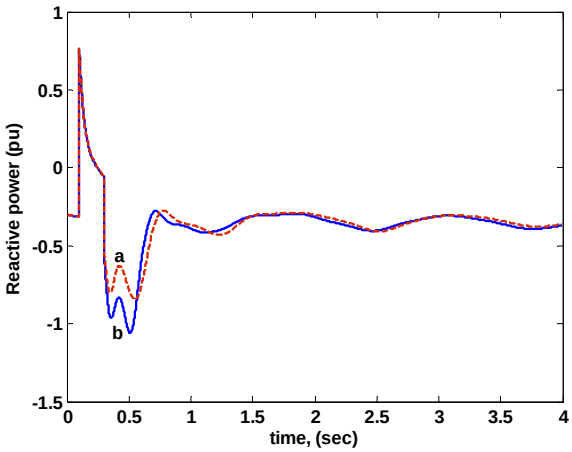

Fig. 20. Post-fault Q-support to the induction generation (a) with susceptance control circuit but no additional control u, and (b) with additional PI control in the susceptance control circuit.

For the weak grid with fault F5, improvement of voltage profile of induction generator is studied when it is equipped with a variable susceptance controller. Figure 21 shows the voltage response when there was no PI with the controller, whereas Figure 22 is the voltage response when PI is incorporated with the controller. It can be seen that without PI controller, the injection of additional susceptance (ΔB) is inadequate. Consequently, terminal voltage recovery is not possible. However, with the incorporation of PI controller, appropriate amount of susceptance is injected thereby terminal voltage of induction generator is restored. Figure 23 shows the amount of injected capacitive susceptance (ΔB) without and with PI controller, and corresponding support of reactive power is shown in Figure 24. So, fast and adequate reactive power support is very important for post-fault voltage recovery in case a squirrel cage induction generator connected to a weak grid. Figure 25 shows the variation of induction generator slip when it is equipped with (a) no susceptance controller, susceptance controller (b) without, and (c) with PI controller. Without susceptance controller slip increases steeply leading to instability with short period of time. With susceptance controller but no PI, oscillations in slip grow rapidly. But incorporation of PI with susceptance controller makes a smooth return of slip to the steady-state value after the fault is cleared.

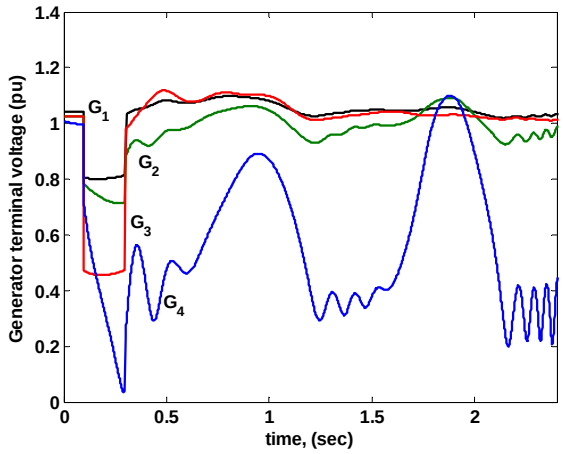

Fig. 21. Terminal voltage response with fault F5 when G4 is an induction generator and equipped with a variable susceptance controller but no PI control (weak grid).

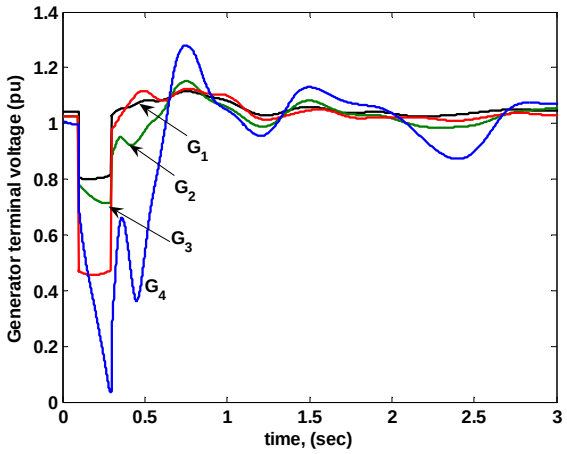

Fig. 22. Terminal voltage response of induction generator with PI regulated variable susceptance controller. Fault scenario is same as Figure 21.

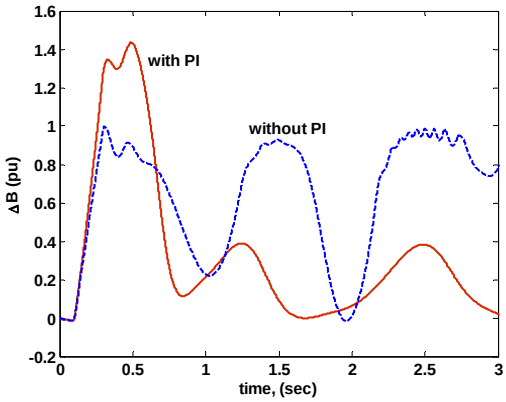

Fig. 23. Variation of injected susceptance (ΔB) in the event mentioned in Figures 21 and 22.

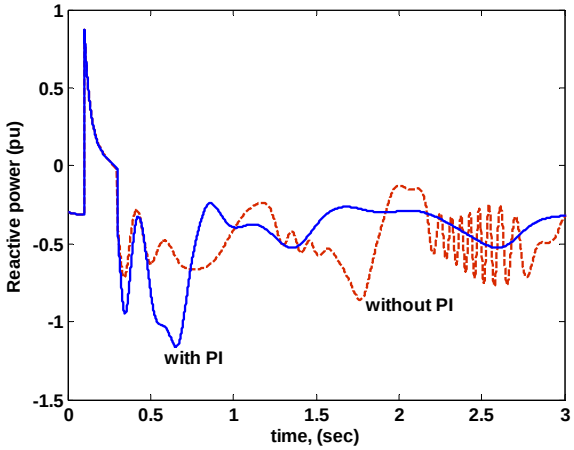

Fig. 24 Reactive power absorbed by the induction generator in the event mentioned in Figures 21 and 22.

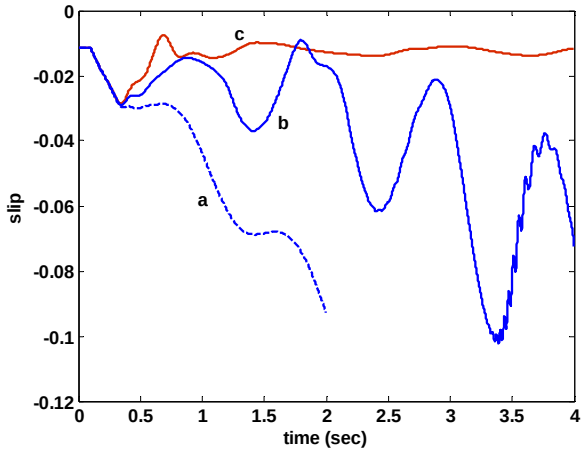

Fig. 25. Variation of induction generator slip with fault F5 (weak grid) (a) without susceptance controller (b) with susceptance controller but no u (c) with PI incorporated susceptance controller.

6. CONCLUSION

Dynamic performance of a multimachine power system including wind turbine driven induction generator has been investigated when it is subjected to grid disturbances. Through a number of simulation studies it is observed that line reactance (or grid strength) has substantial influence on the post fault voltage recovery of the induction generator. Analysis of voltage recovery pattern and corresponding received reactive power support from grid shows that a fast and adequate reactive power support is very important for the smooth recovery of induction generator terminal voltage. Improvement of dynamic performance of system through the introduction of a variable susceptance control circuit located at the

induction generator terminal is investigated. Further enhancement of the dynamic performance with the introduction of additional PI control in the susceptance control circuit has been examined. It has been observed that the fixed-speed induction generators connected to weak grid are very much sensitive to grid faults. Incorporation of a variable susceptance excitation controller can improve dynamic performance substantially. The proposed controller structure is very simple and employs signals local to each machine. It also performs in a robust manner [29], [30].

ACKNOWLEDGMENT

The authors wish to acknowledge the facilities provided at the King Fahd University of Petroleum and Minerals, Dhahran, Saudi Arabia towards this research.

NOMENCLATURE

P_m	wind turbine mechanical power output (pu)
V_w	wind speed (m/sec)
ρ	air density (kg/m^3)
C_p	wind turbine power coefficient
λ	blade tip-speed ratio
β	blade pitch angle
A	blade swept area (m^2)
Ω	mechanical angular velocity of turbine
R	wind turbine blade radius (m)
H_t	wind turbine inertia constant (sec)
H_g	induction generator inertia constant (sec)
H	synchronous generator inertia constant (sec)
K_s	shaft stiffness coefficient (pu/elect.rad)
θ_s	shaft twist angle (rad)
ω_t	wind turbine angular velocity (pu)
ω_r	induction generator angular velocity (pu)
ω_b	base angular velocity (rad/sec)
s	slip of induction generator
T_m	wind turbine rotor mechanical torque (pu)
T_g	mechanical torque applied to the induction generator rotor shaft (pu)
T_e	electromagnetic torque of generator (pu)
T_D	damping torque (pu)
D_i	damping coefficient of turbine (i=t), or generator (i=g) (pu-s/el.rad)
R_s, R_r	stator, rotor resistance (pu)
x_s, x_r	stator, rotor reactance (pu)
x_m, x'	magnetizing, transient reactance (pu)
D, Q	direct and quadrature axis of synchronous reference frame
d, q	direct and quadrature axis of individual machine reference frame
e'_d, e'_q	d and q axis component of voltage behind transient reactance (pu)
Ψ_{dr}, Ψ_{qr}	d and q axis component of rotor flux linkage
T'_o	induction generator rotor open circuit transient time constant (sec)
T'_{do}, T'_{qo}	synchronous generator d and q axis open circuit transient time constants (sec)
E_{fd}	synchronous generator exciter voltage (pu)
K_A, T_A	Gain and time constant of automatic voltage regulator (AVR)
x'_d, x'_q	d and q axis reactance of synchronous generator (pu)
V_{ref}	AVR reference voltage (pu)
δ	transformation angle between machine and network reference frame
Y_{red}	reduced network admittance (Y) matrix
Y_{bf}, Y_{df}	before fault, during fault network Y matrix
Y_{pf}	post-fault network admittance matrix
σ	thyristor conduction angle
B_{TCR}	equivalent inductive susceptance of thyristor controlled reactor (TCR)
X_{TCR}	inductive reactance of TCR
K_{SE}, T_{SE}	gain, time constant of susceptance controller
K_p, K_i	PI controller gains
T_w	washout time constant

REFERENCES

[1] The European Wind Energy Association. Wind Force 12, 2005. A blueprint to achieve 12% of the world's electricity from wind power by 2020, *EWEA Publications*, [Online] Retrieved August 15, 2008, from: http://www.ewea.org/index.php.

[2] Global Wind Energy Council. Accessed on August 15, 2008. http://www.gwec.net.

[3] Anaya-Lara, O., Hughes, F., Jenkins, M.N. and Strbac, G., 2006, Influence of windfarms on power system dynamic and transient stability. *Wind Engineering* 30(2): 107-127.

[4] Senjyu, T., Sakamoto, R., Urasaki, N., Higa, H., Uezato, K. and Funabashi, T., 2006. Output power control of wind turbine generator by pitch angle control using minimum variance control. *Journal of Electrical Engineering Japan* 154(2): 10–18.

[5] Slootweg, J.G., Haan, S.W.H., Polinder, H. and Kling, W.L., 2003. General model for representing variable speed wind turbines in power system dynamics simulations. *IEEE Transactions on Power Systems* 18(1): 144-151.

[6] Causebrook, A., Atkinson, D.J. and Jack, A.G., 2007 Fault ride-through of large wind farms using dynamic breaking resistors. *IEEE Transactions on Power Systems* 22(3): 966-975.

[7] Seyoum, D., Rahman, M.F. and Grantham, C., 2003. Terminal voltage control of a wind turbine driven isolated induction generator using stator oriented field control. In *Proceedings IEEE- 2003 Applied Power Electronics Conference and Exposition,* Florida, USA, pp. 846 -852.

[8] Chompoo-inwai, C., Chitra,Y., Methaprayoon, K. and Lee, W.J., 2004. Reactive compensation techniques to improve the ride-through of induction generators during disturbance. In *Proceedings of the the IEEE 39th IAS Annual Meeting, Industry Application Conference, 3-7 October:* 2044-2050.

[9] Saad-Saoud, Z., Lisboa, M.L., Ekanayake, J.B., Jenkins, N. and Strbac, G., 1998 Application of STACOMs to wind farms. *IEE Proceedings: Generation, Transmission, Distribution* 145(5):511-517

[10] Muyeen, S.M., Takahashi, R., Ali, M.H., Murata T. and Tamura, J., 2006. Stabilization of wind turbine generator system by STATCOM, *IEEJ Transactions on Power Energy* 126-B(10):1073-1082.

[11] Wu, X.G., Arulampalam, A., Zhan, C. and Jenkins, N., 2003. Application of a static reactive power

compensator (STATCOM) and a dynamic braking resistor (DBR) for the stability enhancement of a large wind farm. *Wind Engineering Journal* 27(2): 93-106.

[12] Yang, Z., Shen, C., Zhang, L., Crow, M.L., Dong, L., Pekarek, S. and Atcitty, S., 2001. Integration of a STATCOM and battery energy storage. *IEEE Transactions on Power Systems* 16(2): 254-260.

[13] Muyeen, S.M., Takahashi, R., Ali, M.H., Murata, T. and Tamura, J., 2008. Transient stability augmentation of power system including wind farms by using ECS. *IEEE Trans on Power Systems* 23(3): 1179-1187.

[14] Heier, S., 2007. *Grid Integration of Wind Energy Conversion Systems*, 2nd Edition, John Wiley & Sons, Ltd.

[15] Karari, M., Rosehart, W. and Malik, O.P., 2005, Comprehensive control strategy for a variable speed cage machine wind generator unit. *IEEE Transactions on Energy Conversion* 20(2): 415-423.

[16] Seyoum, D.C., Grantham, M. and Rahman, F., 2003, The dynamic characteristics of an isolated self-excited induction generator driven by a wind turbine. *IEEE Transactions on Industry Applications* 39(4): 936-44.

[17] Salman, S.K. and Teo, A.L.J., 2003. Windmill modeling consideration and factors influencing the stability of a grid-connected wind power based embedded generator. *IEEE Trans on Power Systems* 18: 793-802.

[18] Mei, F. and Pal, B., 2007. Modal analysis of grid-connected doubly fed induction generator, *IEEE Transactions on Energy Conversion* 22(3): 728-736.

[19] Akhmatov, V., 2005. *Induction Generators for Wind Power*, Multi-Science Publishing Company, Ltd.

[20] Shafiu, Anaya-Lara, O., Bathurst, G. and Jenkins, N., 2006. Aggregated wind turbine models for power system dynamic studies, *Wind Engineering*, 30(3): 171-186.

[21] Kundur, P., 1994. *Power System Stability and Control*, EPRI Power System Engineering Series. New York: McGraw-Hill, Inc.

[22] Zhang, J., Dysko, A., O'Reilly, J. and Leithead, W.E., 2008. Modeling and performance of fixed-speed induction generators in power system oscillation stability studies. *Electric Power Systems Research* 78: 1416-1424.

[23] Sauer, P.W., and Pai, M.A., 1998. *Power System Dynamics and Stability.* New Jersey: Prentice Hall.

[24] Feijoo, E. and Cidras, J., 2000. Modeling of wind farms in the load flow analysis. *IEEE Transactions on Power Systems* 15(1): 110-115.

[25] Jayashri, R. and Kumudini Devi, R.P., 2006. Analysis of the impact of interconnecting wind turbine generators to the utility grid. *Wind Engineering* 30(4): 303-316.

[26] Ruiz-Vega, D., Asiaín Olivares, T.I. and Salinas, D.O., 2002. An approach to the initialization of dynamic induction motor models. *IEEE Transactions on Power Systems* 17(3): 747-751.

[27] Ahmed, T., Nishida, K., Soushin, K. and Nakaoka, M., 2005. Static VAR compensator-based voltage control implementation of single-phase self-excited induction generator. *IEE Proceedings: Generation, Transmission, Distribution* 152(2): 145-156.

[28] IEEE Special Stability Controls Working Group. 1994. Static VAR compensator models for power flow and dynamic performance simulation. *IEEE Transactions on Power Systems* 9(1): 229-240.

[29] Rahim, A.H.M.A., Ahsanul Alam, M. and Kandlawala, M.F., 2008. Dynamic performance improvement of an isolated wind turbine induction generator, *Journal of Computer and Electrical Engineering*. (Article in press) doi:10.1016/j.compeleceng. 2008.08.008.

[30] Rahim, A.H.M.A. and Ahsanul Alam, M., 2009. Variable susceptance excitation control for dynamic performance improvement of a stand-alone wind turbine induction generator system. *International Journal of Renewable Energy Technology* 1(1): 1-16.

APPENDIX

Table 1. Generation and load data for the base case (from load flow solution).

Bus #	Generation		Load	
	P_g, MW	Q_g, MVAR	P_L, MW	Q_L, MVAR
1	37.55	23.94	-	-
2	105	16.107	-	-
3	50	19.603	-	-
4	60	4.098	-	-
5	-	-	77.5	30
6	-	-	52.5	25
8	-	-	72.5	27
12	-	-	48.75	15

In case of induction generator, the injected reactive power at the generator terminal (bus 4) is 35.23 MVar.

Table 2. Line data.

From bus	To Bus	R (pu)	X (pu)	B/2 (pu)
1	7	0	0.05	0
2	9	0	0.05	0
4	10	0	0.05	0
3	11	0	0.05	0
11	12	0.018	0.1167	0.0175
11	5	0.009	0.10	0.035
5	10	0.009	0.1167	0.035
10	6	0.009	0.135	0.035
6	9	0.009	0.1075	0.035
9	8	0.009	0.11	0.049
8	7	0	0.1333	0.035
7	5	0.009	0.1333	0.035